Int. J. Electrochem. Sci., 6 **(2011)** 2688 - 2709

International Journal of
ELECTROCHEMICAL
SCIENCE
www.electrochemsci.org

Amperometric and Impedimetric H_2O_2 Biosensor Based on Horseradish Peroxidase Covalently Immobilized at Ruthenium Oxide Nanoparticles Modified Electrode

Arun Prakash Periasamy, Shan Wei Ting and Shen-Ming Chen[*]

Department of Chemical Engineering and Biotechnology, National Taipei University of Technology, No.1, Section 3, Chung-Hsiao East Road , Taipei 106, Taiwan (R.O.C).
[*]E-mail: smchen78@ms15.hinet.net

Received: 3 May 2011 / *Accepted:* 6 June 2011 / *Published:* 1 July 2011

In this work, Ruthenium oxide nanoparticles (RuNPs) were electrochemically deposited on a glassy carbon electrode (GCE) surface using $RuCl_3$. nH_2O as a precursor. The model redox enzyme, horseradish peroxidase (HRP) was covalently immobilized at the RuNPs modified electrode surface using Chitosan–glutaraldehyde (Chi–GAD) cross-linking. The surface morphology of RuNPs, HRP and HRP/Chi–GAD/RuNPs films were investigated using scanning electron microscopy (SEM) and atomic force microscopy (AFM) studies. From the SEM and AFM results the average size of the RuNPs was calculated as 60–160 nm. UV-visible absorption spectra of HRP and HRP/Chi–GAD/RuNPs films displayed a soret band at 406 nm and thus the immobilized HRP retains its native structure at Chi–GAD/RuNPs film. Electrochemical impedance spectroscopy (EIS) results confirmed the rapid electron transfer process occurring at the composite film surface. The electron transfer resistance (R_{et}) values observed at the composite film surface varied linearly between 5.92 $x10^{-5}$ M–6.15 x 10^{-4} M H_2O_2 additions, which validates the efficient impedimetric H_2O_2 quantification. The composite film also showed excellent amperometric i–t response towards H_2O_2 in the linear concentration range between 5.09 x 10^{-3} M–1.5 x 10^{-2} M. The developed HRP/Chi-GAD/RuNPs biosensor was highly selective towards H_2O_2 and acceptable H_2O_2 recovery was achieved in the contact lens cleaning solution.

Keywords: Ruthenium oxide nanoparticles, chitosan, glutaraldehyde, hydrogen peroxide, electrocatalysis.

1. INTRODUCTION

Hydrogen peroxide (H_2O_2) has been an extensively studied compound of interest since it acts as a central oxygen metabolite and it plays a vital role in biological systems [1]. H_2O_2 is also an

essential component of plant tissues and it is involved in the regulation of plant metabolism, defense and acclimatory processes and gene expression [2]. Owing to the excellent oxidizing and antibacterial property, H_2O_2 has been largely used in industries as an oxidizing agent [3], antibacterial agent [4] and bleaching agent [5]. Besides these applications the significance of analytical measurement of exhaled H_2O_2 and its exploitation as a potent diagnostic tool and non-invasive biomarker for clinical applications have been to date reviewed by Stolarek *et al.* [6]. The immense applications of H_2O_2 in diverse fields emphasized the demand to explore a simple, cost-effective, easily portable tool with adaptable measurement protocol for H_2O_2 quantification. However, the important analytical requirements for rapid H_2O_2 monitoring such as high sensitivity, reliability and operational simplicity [7] were not satisfied with the available conventional approaches [8-13]. In addition, these conventional approaches are experiencing serious shortcomings like cost-effectiveness and time-consuming sample preparations.

On the other hand, amperometric horseradish peroxidase (HRP) based biosensors have been extensively employed now a days in direct H_2O_2 determinations because of their unique advantages such as high sensitivity, good stability, the availability of wide variety of disposable electrodes, inexpensive and compact instrumentation techniques [14–15]. In such peroxidase based biosensors, H_2O_2 is electroenzymatically reduced at low over potential due to the direct electron transfer between the electrode surface and HRP [16]. The immense advancements made in the nanotechnology field in recent times have encouraged the utilization of nanomaterials in enzyme based biosensors for achieving rapid direct electron transfer and for designing new generation biosensors with high sensitivity and stability [17]. So far, the direct electron transfer of HRP has been reported at nanomaterial surfaces such as gold nanoparticles (AuNPs) [18], gold nano wire array electrodes [19], cadmium sulphide (CdS) nanorods [20], and carbon nanotubes (CNTs) [21-22]. Apart from these nanomaterials, nanostructured metal oxides and their composites have also been utilized for promoting the direct electron transfer of HRP since they possess unique characteristics like high sensitivity, good biocompatibility, low-cost, excellent electrochemical activity [23] and the rapid response associated with their specific metal oxide nanostructures [24]. Hitherto, the direct electron transfer of HRP has been reported at nanostructured metal oxide surfaces such as zinc oxide (ZnO) [25–26], titanium dioxide (TiO_2) [27], mesoporous TiO_2 and tin oxide (SnO_2) [28], SnO_2 nanorods [29], SiO_2 nanoparticles [30], nanostructured cerium oxide (CeO_2) [31], nickel oxide nanoparticles (NiO NPs) [32], polyquaternium-manganese oxide nanosheets [33], and Zirconia nanocomposites [34–35].

The sensitivity and stability of a biosensor could be improved by choosing suitable enzyme immobilization matrix and by adapting better enzyme immobilization strategies. The diverse strategies employed in HRP based biosensors include physical entrapment in sol-gels [36–37], layer-by-layer technique [38], and covalent immobilization via crosslinking agents [39]. Among these immobilization techniques, good stability of the biosensor could be achieved by covalent immobilization technique. Owing to the unique properties of chitosan (Chi) such as biocompatibility, nontoxicity, physiological inertness, remarkable affinity to proteins [40], and due to the presence of large number of free amino groups, Chi has been used as a cross linking agent in HRP based biosensors [41, 42]. Similarly, glutaraldehyde (GAD) is a well known bifunctional agent, which could act both as a crosslinker and surface activating agent [43].

From the thorough view of literature we believe that nanostructured metal oxide modified surfaces could be prominent matrices for HRP immobilization. However, to the best of our knowledge, no one has reported the direct electron transfer of HRP at ruthenium oxide nanoparticles (RuNPs) modified surfaces. RuNPs with several advantages like strong adhesion, longer life in erosion tests, fine patterning, and well-defined interface along with good biocompatibility for enzymes, it has been successfully employed for immobilizing ascorbate oxidase [44]. Recently, Peng *et al.* have reported a highly sensitive, selective RNA biosensor with femto molar detection limit using RuNPs [45]. Kotzian *et al.* have developed an amperometric flow injection analysis (FIA) based biosensor for H_2O_2, glucose and hypoxanthine detections using RuNPs modified SPE electrodes [46]. Due to the excellent biocompatibility and good affinity of RuNPs modified surfaces for biomolecules, we attempt to develop a HRP based biosensor using RuNPs. We report a highly selective amperometric H_2O_2 biosensor based on HRP using ruthenium oxide nanoparticles (RuNPs) for the first time. The electrochemical deposition of RuNPs on a glassy carbon electrode surface helps to prepare uniform nano metal oxide film with well defined spherical shaped RuNPs. The prepared RuNPs has been utilized as a novel platform to immobilize HRP via Chi-GAD crosslinking. The developed biosensor showed rapid response towards H_2O_2 with high sensitivity and selectivity. The proposed HRP/Chi-GAD/RuNPs film has been employed for both amperometric and impedimetric H_2O_2 quantifications.

2. EXPERIMENTAL

2.1. Reagents

Peroxidase, from horseradish, type VI-A and chitosan from crab shells, minimum 85 % deacetylated were purchased from Sigma and used as received. 25 wt. % glutaraldehyde (GAD) solution in water was obtained from Sigma-Aldrich. Ruthenium (III) chloride was purchased from Aldrich. H_2O_2 (30%) was obtained from Wako pure chemical Industries, Ltd. The supporting electrolytes used in this study are pH 2 aqueous solution and 0.05 M pH 7 phosphate buffer solutions (PBS). PBS was prepared using 0.05 M Na_2HPO_4 and NaH_2PO_4 solutions. All the reagents used in this work were of analytical grade and all aqueous solutions were prepared using doubly distilled water. Prior to each experiment, the experimental solutions were deoxygenated with pre-purified N_2 gas for 10 min and the N_2 tube was kept above the solutions to maintain an inert atmosphere.

2.2. Apparatus

Cyclic voltammetry (CV) experiments were carried out using CHI 1205a work station. A conventional three electrode cell containing 4 ml of freshly prepared PBS was used for electrochemical studies. GCE with an electrode surface area of 0.079 cm^2 was used as working electrode. Pt wire with 0.5 mm diameter was used as counter electrode and all the potentials were referred with respect to standard Ag/AgCl reference electrode. UV–vis absorption spectroscopy measurements were carried out using Hitachi U-3300 spectrophotometer. EIM6ex ZAHNER (Kroanch, Germany) was used for

electrochemical impedance spectroscopy (EIS) and impedimetric catalysis studies. Surface morphology studies were carried out using Hitachi S-3000 H scanning electron microscope (SEM) and Being nano-instruments CSPM 4000, atomic force microscope (AFM).

2.3. Preparation of Chi-GAD and HRP solutions

To prepare 0.5 % Chitosan solution, weighed amount of Chitosan flakes were dissolved in 10 ml of 2 M acetic acid and the resulting solution was ultrasonicated well until the Chitosan flakes were completely dissolved. Then, 50µl of 0.25% GAD aqueous solution was added into the Chitosan solution. The reaction between Chitosan and GAD depends upon the solution pH and less than an hour was sufficient for the completion of the reaction [47]. In order to allow the crosslinking reaction to occur, we constantly stirred the Chitosan-GAD mixture for 30 min. During the crosslinking reaction, the free pendant amine groups of chitosan polymer interacts with the aldehydic group of the glutaraldehyde to form stable imine bonds as a result of the resonance established with adjacent double ethylenic bonds [47]. The finally obtained Chitosan-GAD solution was thus named as Chi-GAD and it was used as cross-linking agent to immobilize HRP at RuNPs modified electrode surface. Similarly, 2 mg ml^{-1} HRP solution was prepared in PBS. The Chi-GAD and HRP solutions were stored at 4 °C when not in use.

2.4. Fabrication of HRP/Chi-GAD/RuNPs modified GCE

The electrochemical technique is more beneficial for RuNPs deposition since we could control the film thickness by optimizing the number of deposition cycles. In particular, we can avoid the agglomeration of the nanoparticles in solution phase. However, the other parameters like precursor concentration, solution pH may influence the RuNPs deposition. So we used an optimum precursor concentration of 1 mM $RuCl_3$ and the solution pH was maintained at 2, respectively. The supporting electrolyte solution was 0.01 M KCl. Before carrying out RuNPs deposition, the GCE surface was polished to a mirror finish on a clean Buehler polishing cloth using 0.05 µm alumina slurry. In order to remove the loosely adsorbed alumina particles the polished GCE surface was washed and ultrasonicated in doubly distilled water for 10 min. Finally, the clean GCE surface was dried in air for few minutes and it was transferred to an electrochemical cell with 1 mM $RuCl_3$ in 0.01 M KCl supporting electrolyte solution. As shown in Fig. 1, 30 consecutive cyclic voltammograms were performed in the potential range between -0.3 and 1.2 V at the scan rate of 100 mV s^{-1}.

During the positive potential scan, two anodic peaks appeared at 0.480 V and 0.965 V. Their corresponding reduction peaks were observed at 0.84 V and 0.136 V in the negative potential scan. As indicated by the arrows in Fig.1, both the anodic and cathodic peaks observed at 0.480 V and 0.136 V increased gradually with the increase in number of potential scanning cycles between 1 and 30. The reduction of Ru (III) starts at 0.3 V.

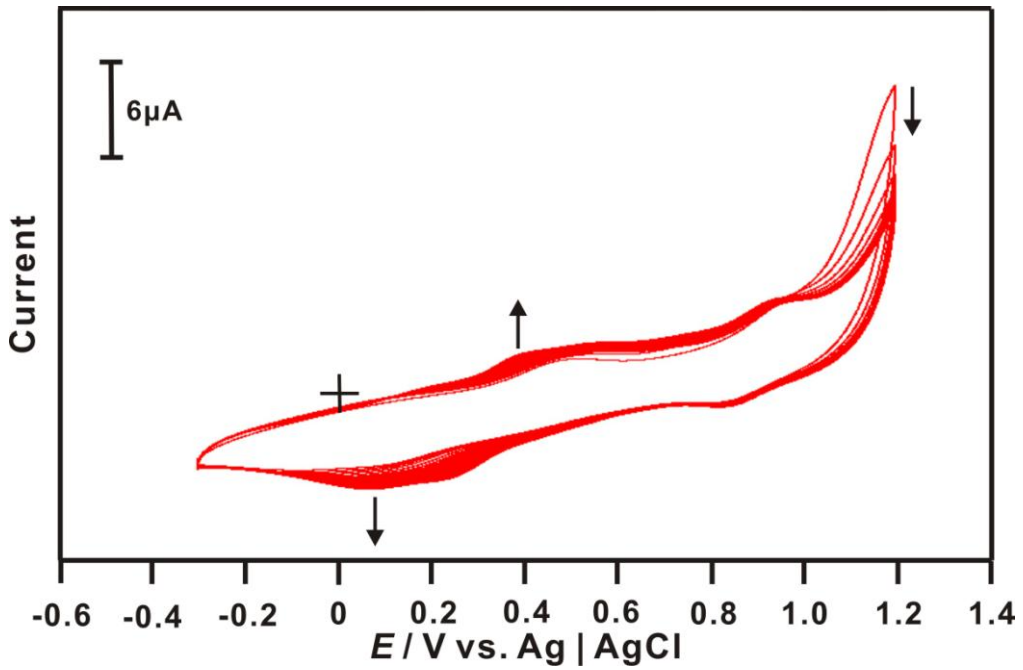

Figure 1. 30 consecutive cyclic voltammograms recorded at GCE kept immersed in 1 mM $RuCl_3$ containing 0.01 M KCl solution. Scan rate used is 100 mV s^{-1}.

During each negative potential scan this reduction peak continues to grow between 0.3 V and -0.1 V, which leads to the deposition of nano-sized Ru particles on the GCE surface. The deposited nano sized Ru film will be oxidized to hydrous oxides (RuO_x. nH_2O) and hydroxyl Ru (VI) species in the positive potential scan which is obvious from the appearance of the oxidation peaks at 0.480 V and 1.1 V. Similar results have been reported in literature for the deposition of hydrous RuO_x. nH_2O films [48-49]. The appearance of characteristic Ru redox peaks in the investigated potential range confirmed the deposition of RuNPs on the GCE surface. Then the RuNPs modified GCE surface was washed gently with water to remove the loosely adsorbed RuNPs. 10 µl of Chi-GAD solution was drop casted on the RuNPs film surface and dried at 25°C for 90 min. The Chi-GAD/RuNPs/GCE surface was then utilized for immobilizing HRP. About 10 µl of 2 mg ml^{-1} HRP solution was drop casted carefully on the Chi-GAD/RuNPs/GCE surface and dried at 25°C for 1 h. Thus obtained HRP/Chi-GAD/RuNPs/GCE was washed gently with water and stored at 4 °C. For comparison, RuNPs and Chi-GAD/RuNPs/GCEs were also prepared.

3. RESULTS AND DISCUSSION

3.1. Investigation of electrochemical behavior of various film modified GCEs *using CV studies*

Electrochemical behavior of RuNPs, Chi-GAD/RuNPs and HRP/Chi-GAD/RuNPs film modified GCEs were investigated using CV in N_2 saturated PBS at the scan rate of 20 mV s^{-1}. As shown in Fig.1 (a), RuNPs/GCE exhibited a quasi-reversible redox peak at a formal potential (E°′) of

0.239 V. This E°′ value is close to the E°′ value of 0.25 V reported for the [Ru^{III} – O]/[Ru^{IV}–O] redox couple [50].

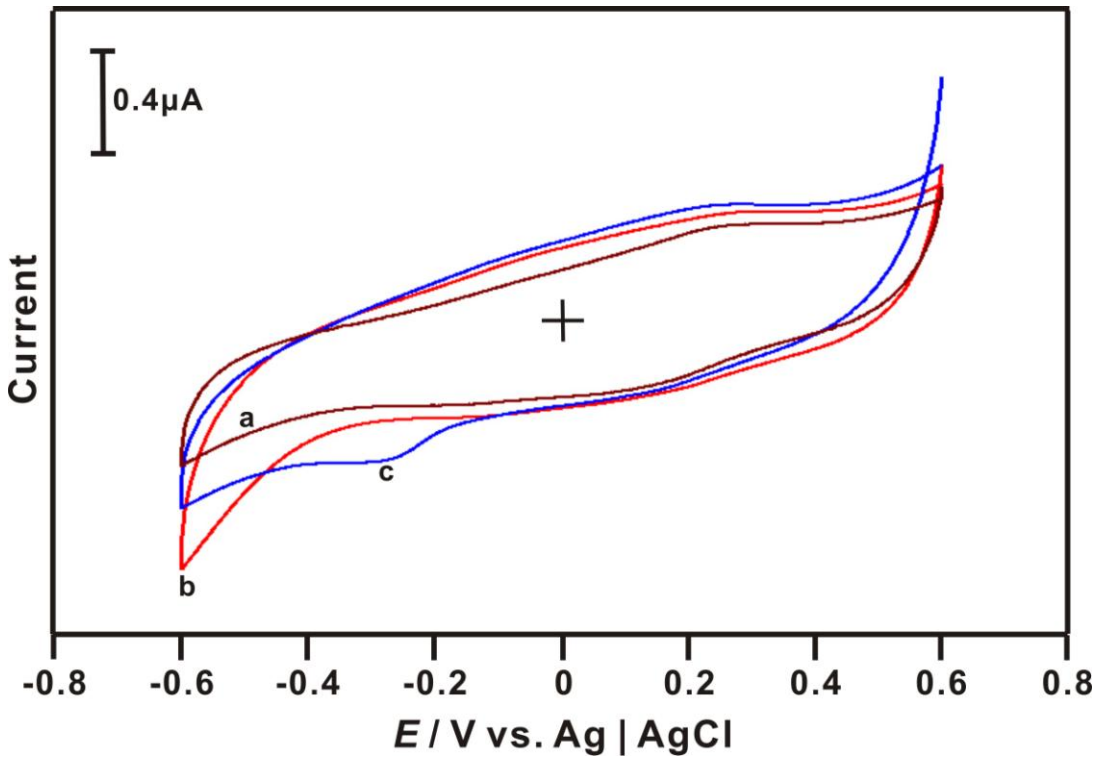

Figure 2. Cyclic voltammograms of (a) RuNPs and (b) Chi-GAD/RuNPs and (c) HRP/Chi-GAD/RuNPs film modified GCEs in N_2 saturated PBS at the scan rate of 20 mV s^{-1}.

This result confirmed the deposition of RuNPs on the GCE surface. With no further shift in the peak potential and E°′ values, Chi-GAD/RuNPs/GCE displayed a similar redox couple with enhanced peak currents (Fig. 2(b)). On the other hand, the HRP/Chi-GAD/RuNPs/GCE showed an enhanced cathodic peak at -0.283 V and a slightly enhanced anodic peak at 0.189 V. The E°′ value for this redox couple is -0.047 V, which is closer to the E°′ value of 0.06 ± 4 V vs. Ag/AgCl reported at HRP/Nafion-cysteine/Au electrode [51] and it is 53 mV more positive than the E°′ value reported at HRP/$CaCO_3$–AuNPs/ATP/Au in PBS (pH=7) [52]. This result validates the direct electron transfer between the HRP and the electrode surface. The possible reason for the direct electron transfer might be the presence of the HRP molecules at the closer vicinity of the electrode surface due to the crosslinking reaction between HRP and Chi-GAD. Besides, the large surface area and good conductivity of RuNPs, the several nano-pores available at the RuNPs modified surface helps to accommodate more number of HRP molecules in the close proximity of the electrode surface. As long as a better contact is established between the HRP molecules and the transducer surface the direct electron transfer will occur at the modified electrode surface. Furthermore, the effect of scan rate on the redox behavior of HRP/Chi-GAD/RuNPs/GCE was also investigated in N_2 saturated PBS. The cyclic voltammograms obtained at HRP/Chi-GAD/RuNPs/GCE in N_2 saturated PBS at different scan rates are shown in Fig. 3.

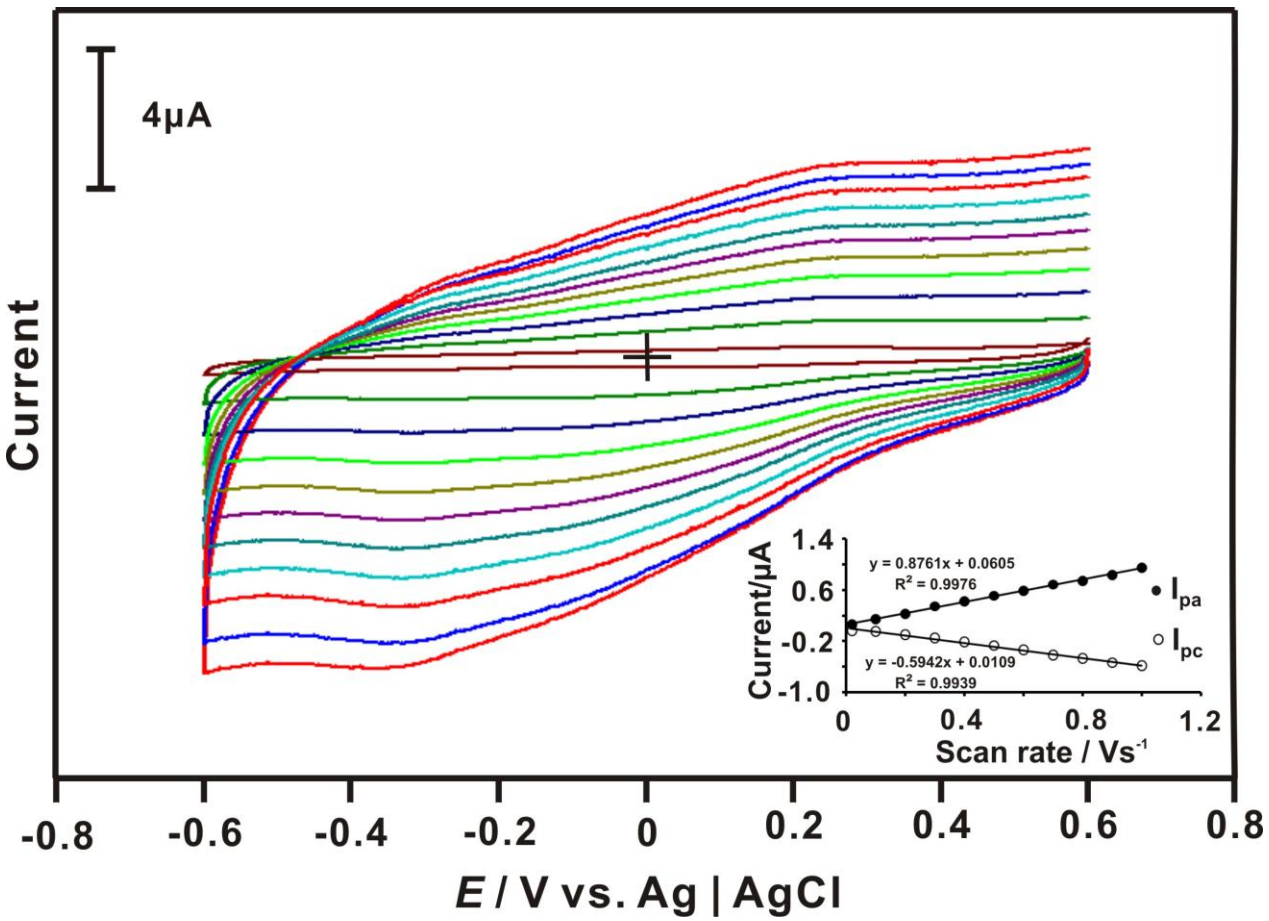

Figure 3. Cyclic voltammograms obtained at HRP/Chi-GAD/RuNPs/GCE in N_2 saturated PBS at different scan rates. The scan rates from inner to outer are 20, 100, 200, 300, 400, 500, 600, 700, 800, 900 and 1000 mV s^{-1} respectively. The inset (a) is the plot of peak currents (I_{pa} and I_{pc}) vs. scan rates (Vs^{-1}).

The peak currents (I_{pa} and I_{pc}) vs. scan rates plot shown in Fig. 3 inset exhibits a linear relationship with R^2 = 0.9976 and 0.9939, respectively. Both I_{pa} and I_{pc} increased linearly with increase in scan rates between 20 to 1000 mV s^{-1}, thus the redox process occurring at HRP/Chi-GAD/RuNPs/GCE is surface-confined. The surface coverage (Γ) value of HRP at HRP/Chi-GAD/RuNPs/GCE have also been calculated using the following equation,

$$\Gamma = Q/nFA \qquad (1)$$

Where, Q is the charge, n is the number of electrons involved, F, Faraday current and A, electrode area. Where, the number of electrons transferred is 1 for $Fe^{III/II}$ redox reaction of HRP. The Γ value of HRP at HRP/Chi-GAD/RuNPs/GCE is calculated to be about 5.19 x 10^{-11} mol cm^{-2} and it is higher than the Γ value of HRP obtained at other HRP modified electrodes reported previously [53-56]. The higher Γ value of HRP at HRP/Chi-GAD/RuNPs/GCE could be attributed to the large surface area and the porous nature of RuNPs which helps for the efficient loading of HRP. However, the HRP

present at the close proximity of the electrode surface could only establish a better contact with the electrode surface and would be involved in electron transfer.

3.2. The effect of pH

The influence of pH on the redox behavior of HRP/Chi-GAD/RuNPs/GCE in various buffer solutions (pH, 1, 4, 7, 9, 11 and 13) were also investigated in this study. The pH study results are shown in Fig.4.

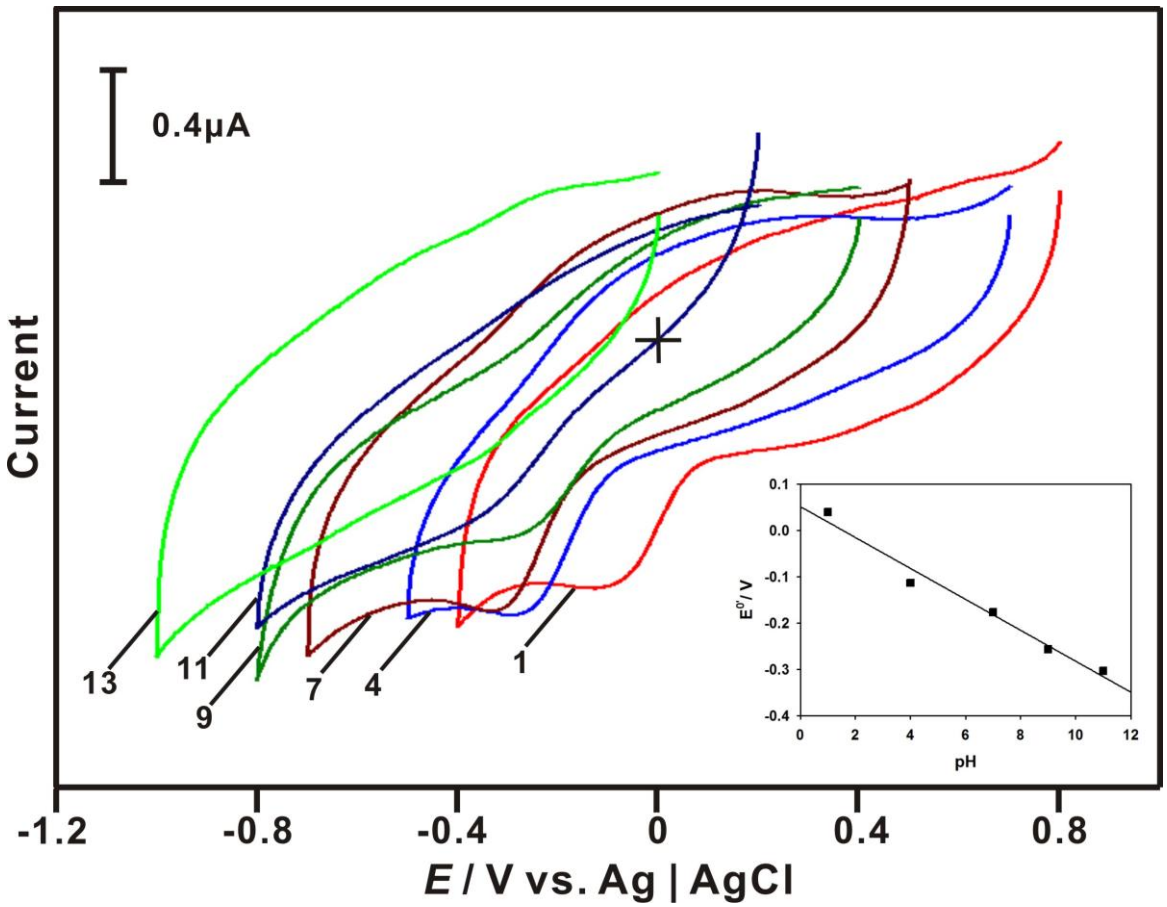

Figure 4. The effect of pH on the redox behavior of HRP/Chi-GAD/RuNPs/GCE in various buffer solutions with pH: 1, 4, 7, 9, 11 and 13, respectively. The inset is E°' vs. pH plot.

A well-defined quasi-reversible redox peaks corresponding to $Fe^{(III/II)}$ redox process of HRP was observed in the pH range between 1 and 11. The redox peak currents increased with increase in pH of the solution, i.e. especially up to pH 7 and thereafter they decreased gradually and the redox peaks were disappeared in pH 13. This might be due to the loss of enzyme activity in the higher pH solution. As shown in Fig. 4 inset, the E°′ of the $Fe^{(III/II)}$ redox couple of HRP exhibits a linear dependence on pH. The E°′ values showed a negative shift with increase in pH with a slope value of -33 mV pH^{-1}, respectively. This slope value is smaller than the theoretical value of -59 mV pH^{-1} for an

equal number of electron and proton transfer process. However, it is close to the slope of −37.8 $mVpH^{-1}$ reported at HRP/DDAB–$HIMIMPF_6$ film [53]. Similar low slope values have also been reported at other HRP modified electrodes [57–59].

3.3. UV-vis absorption spectroscopy study

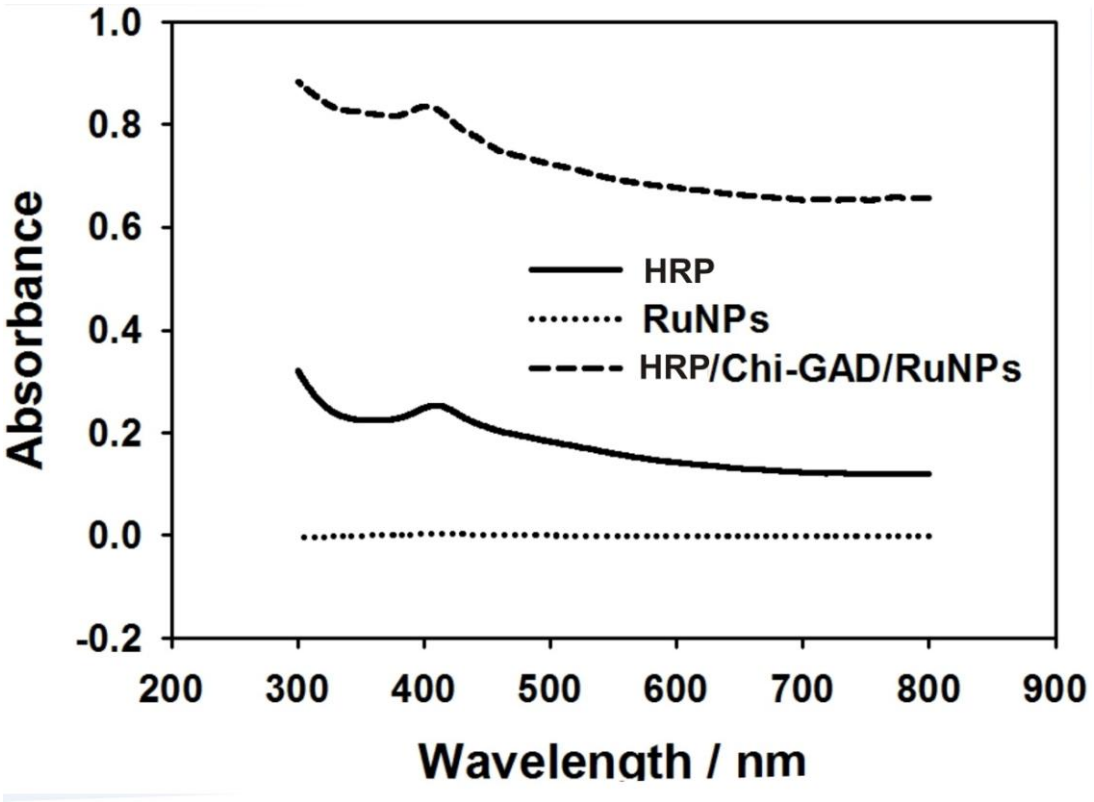

Figure 5. (a) UV-vis absorption spectra of RuNPs (dotted line), HRP (bold continuous line) and HRP/Chi-GAD/RuNPs (dashed line) films.

It is well known that from the exact location and from the shift in position of the soret absorption band it is possible to confirm the denaturation of heme proteins at the immobilization matrix. In this study, UV-visible absorption spectroscopy has been used as an effective tool to confirm whether the HRP retains its native structure at Chi-GAD/RuNPs matrix. Fig. 5 shows the UV-visible absorption spectra of RuNPs, HRP and HRP/Chi-GAD/RuNPs films. No characteristic absorption bands were observed in the absorption spectra of RuNPs film in the wavelength range between 300 and 800 nm. On the other hand, the heme bands of HRP casted film and HRP in buffer will be observed at 404 nm and 403 nm, respectively [60]. In the present study, the Soret band of both HRP and HRP/Chi-GAD/RuNPs casted films are observed at 406 nm which is close to the heme bands of HRP reported in the literature. The above discussed UV-visible absorption spectra results reveal that HRP retains its native structure at the Chi-GAD/RuNPs matrix. Thus the Chi-GAD/RuNPs matrix provides good biocompatibility for the immobilized HRP.

3.4. Surface morphological characterizations using SEM and AFM studies

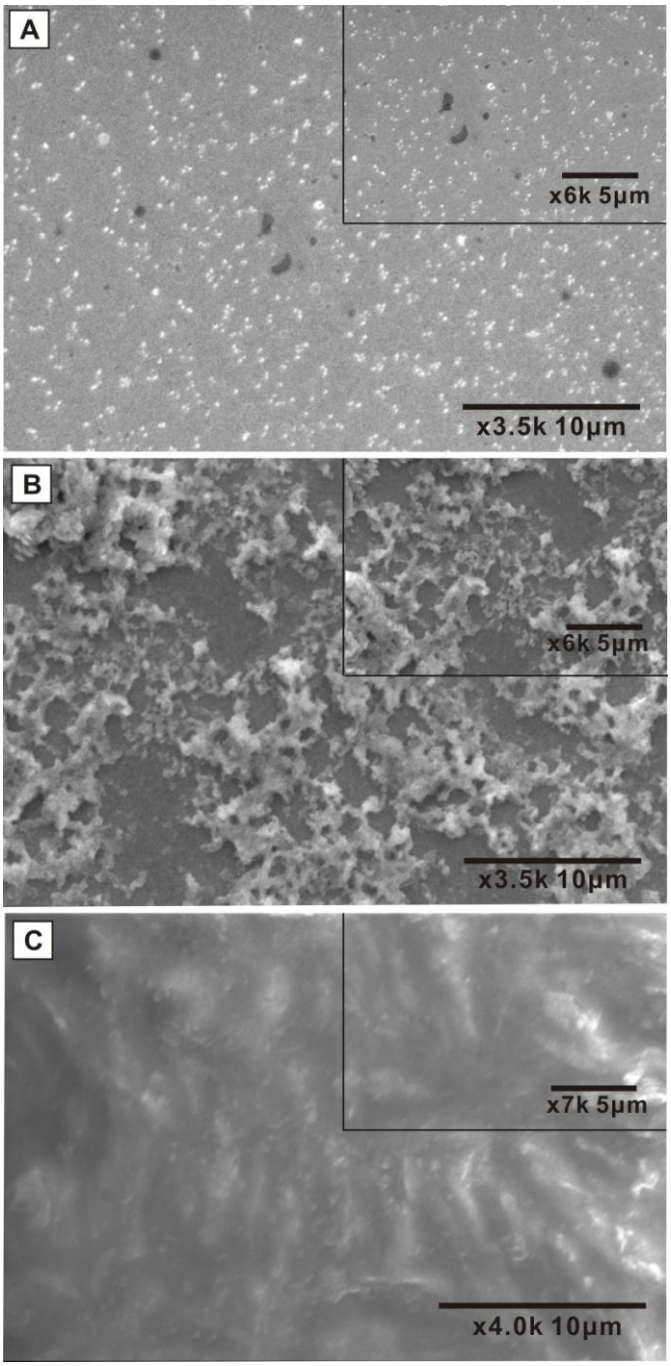

Figure 6. SEM images of (A) RuNPs, (B) HRP and (C) HRP/Chi-GAD/RuNPs films captured at 10 µm magnifications. The insets in (A-C) are the SEM images of RuNPs, HRP and HRP/Chi-GAD/RuNPs films captured at 5 µm magnifications.

SEM study was employed to investigate the surface morphology of RuNPs, HRP and HRP/Chi-GAD/RuNPs films. The SEM image of RuNPs film at 10 µm and 5 µm magnifications are shown in Fig. 6(A) and in the inset. In both these images, several bright, spherical shaped particles are

evenly distributed throughout the film surface and no significant agglomeration of RuNPs is observed here.

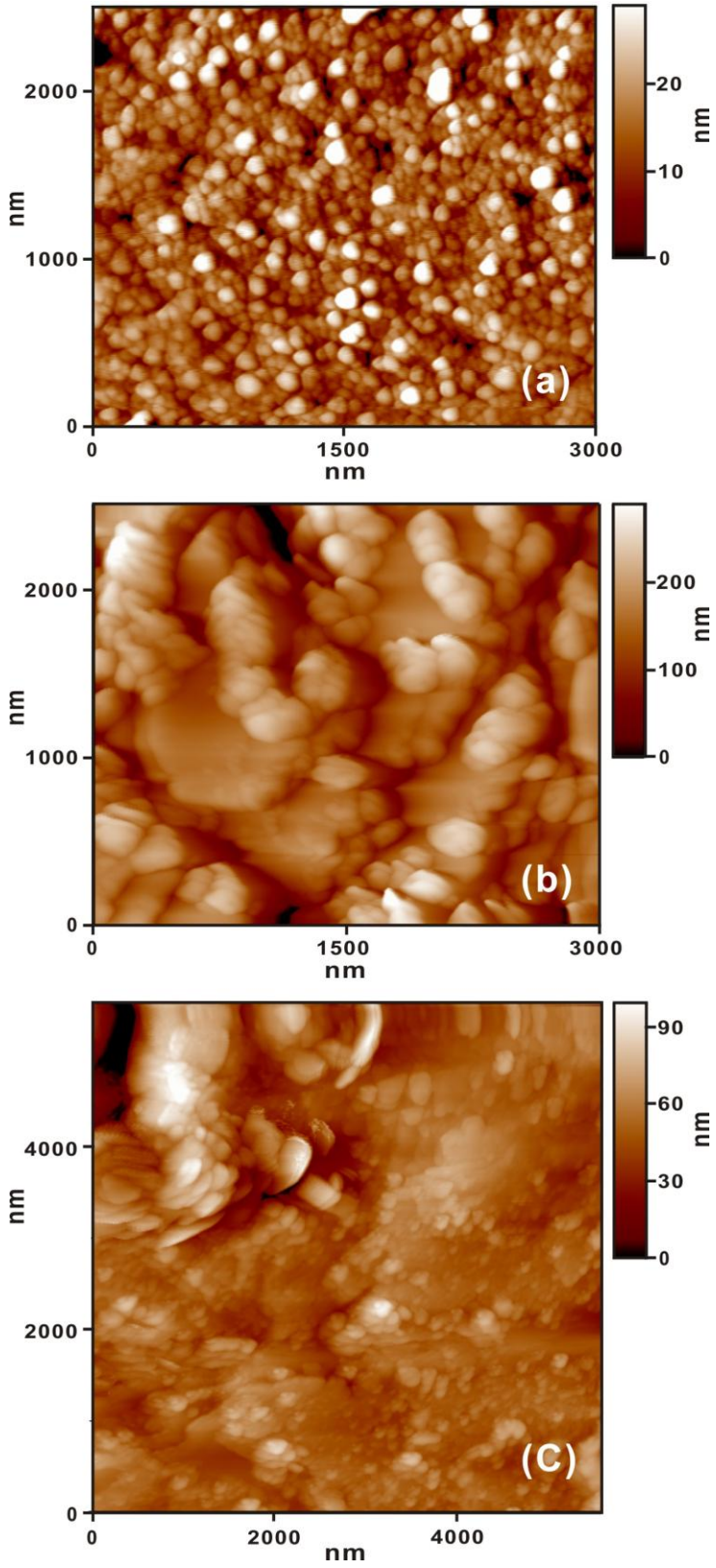

Figure 7. AFM images of (a) RuNPs, (b) HRP and (c) HRP/Chi-GAD/RuNPs films.

This may be attributed to the steady cycle wise electrochemical deposition of RuNPs on the electrode surface. The RuNPs size was between 60 – 160 nm, respectively. The SEM image of HRP captured at 10 µm and 5 µm magnifications are shown in Fig. 6 (B) and in the inset. Unlike RuNPs film, the HRP film surface possesses several bright globular structures.

As can be seen from Fig. 6 (B) the entire film surface is not evenly covered by the HRP globules. Instead, they have formed several big and small clusters validating that bare electrode surface is not efficient for HRP immobilization. On the other hand, the SEM image of HRP/Chi-GAD/RuNPs captured at 10 µm and 5 µm magnifications depicts a more uniform surface morphology as shown in Fig. 6 (C) and in the inset.

The HRP globules and bright RuNPs are covered well by a thick wrinkled Chi-GAD film which authenticates the good affinity of HRP towards Chi-GAD/RuNPs matrix. Further, the crosslinking of HRP with the Chi-GAD layer allows the HRP to immobilize well at the RuNPs modified electrode surface.

The SEM results confirmed the formation of RuNPs, HRP and HRP/Chi-GAD/RuNPs films and clearly demonstrate that RuNPs modified electrode surface is more efficient for HRP immobilization.

Fig. 7 (a) shows the AFM image of RuNPs film, where several bright, spherical shaped RuNPs in the size range of 60 -160 nm are uniformly distributed throughout the film surface. No notable RuNPs clusters or their agglomerates were observed here.

The well-defined spherical shape of RuNPs as well as their uniform distribution on the electrode surface without any significant agglomeration could be attributed to the controlled deposition of RuNPs by CV technique.

Rather than other conventional deposition methods, the utilization of CV technique in this study could have offered better distribution of nanoparticles on the substrate surface.

Further, the electrochemical deposition is more advantageous than other traditional method of RuNPs preparation in the sense that it doesn't require any capping agents, chemical treatments or tedious temperature controlled measurements while the film thickness could be optimized directly by controlling the number of potential sweeping cycles, precursor and electrolyte concentrations and scan rates.

Further, the black colored region found in the AFM image of RuNPs confirmed the presence of nano-voids which could allow the more efficient loading of HRP molecules. Unlike the well-defined spherical shape of RuNPs, the AFM image of HRP film shown in Fig. 7(b) possess both flattened and globular structures. Whereas the AFM image of HRP/Chi-GAD/RuNPs film shown in Fig. 7(c) possess more uniform surface morphology.

The bright spherical shaped RuNPs as well as flake and globular shaped HRP molecules are embedded in the Chi-GAD film.

Further, the thickness of the composite film (90 nm) is higher than the thickness of RuNPs film (20 nm), which validates the formation of HRP/Chi-GAD film above the RuNPs surface. Therefore, the above mentioned AFM results confirmed the immobilization of HRP at the composite film surface.

3.5. Investigation of electrochemical behavior of various film modified electrodes using EIS studies

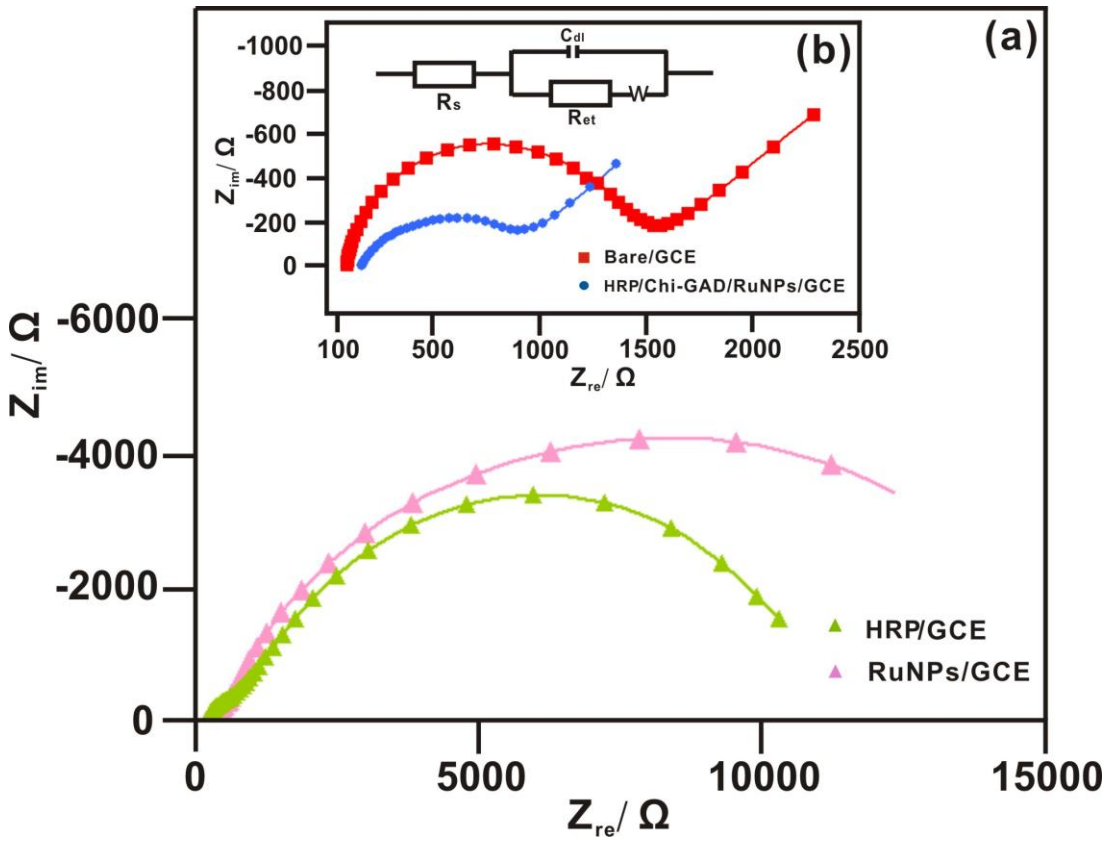

Figure 8. (a) EIS of HRP/GCE and RuNPs/GCE recorded in PBS containing 5 mM $Fe(CN)_6^{3-}/Fe(CN)_6^{4-}$. Amplitude: 5 mV, frequency: 100 mHz to 100 kHz. (b) EIS of bare/GCE and HRP/Chi-GAD/RuNPs/GCE recorded under similar conditions as that of (a). The EIS data obtained at above said modified electrodes were fitted using the Randles equivalence circuit given in the inset of Fig. 8 (b).

Fig. 8 (a) shows the real and imaginary parts of the impedance spectra represented as Nyquist plots (Z_{im} vs. Z_{re}) for HRP and RuNPs/GCEs recorded in PBS containing 5 mM $Fe(CN)_6^{3-/4-}$. Similarly, Fig. 8 (b) displays the Nyquist plot of bare and HRP/Chi-GAD/RuNPs/GCEs recorded under similar conditions as that of (a). Inset in Fig. 8 (b) is the Randles equivalence circuit model used for fitting the EIS data of the above mentioned electrodes. From the best fitted model, we have calculated the electron transfer resistance (R_{et}), double layer capacitance (C_{dl}), Wardburg impedance (W) and electrolyte resistance (R_s) values. It is clear from Fig. 8 (a) and (b) that all modified electrodes exhibit well defined semicircles in the investigated frequency range. Compared with bare and HRP/GCEs, an enlarged semicircle is found in the Nyquist plot of RuNPs/GCE which confirms the deposition of RuNPs on GCE surface. Here, the closely distributed RuNPs layer may hindered the mobility of Fe $(CN)_6^{3-/4-}$ ions and which could have slow down the electron transfer. On the other hand, HRP/GCE too exhibits an enlarged semicircle than bare/GCE, which also reveals a sluggish electron transfer. However, the diameter of the semicircle portion of HRP/GCE is slightly smaller than that of RuNPs/GCE. The possible reason for the poor electron transferring efficiency of HRP/GCE may be

due to the inaccessibility of its heme centre for direct electron transfer, since it is deeply buried inside the polypeptide chain. Amongst all the electrodes we studied, HRP/Chi-GAD/RuNPs/GCE exhibits a smallest semicircle with a lowest R_{et} value of 517.3 Ω. In particular, the R_{et} value of the composite film is significantly smaller than the R_{et} value of bare/GCE, which is about 1.28 K Ω, respectively. This result confirms the more rapid electron transfer process occurring at the composite film surface. The reason for the rapid electron transfer across the composite film surface may be due to the covalent crosslinking achieved by Chi-GAD which helps the HRP to establish better contact with the electrode surface. Furthermore, the large surface area, good conductivity of RuNPs and the excellent biocompatibility of Chi-GAD film offers a suitable microenvironment for the HRP to undergo rapid electron transfer kinetics. Thus EIS results substantiate that RuNPs could be a good platform for immobilizing proteins.

3.5.1. Impedimetric biosensor for H_2O_2 determination using HRP/Chi-GAD/RuNPs *film modified electrode*

In order to develop an impedimetric biosensor, we performed EIS measurements at the HRP/Chi-GAD/RuNPs/GCE in the presence of various H_2O_2 concentrations. The obtained Nyquist plots are shown in Fig. 9. In the Nyquist plots, the semicircles from inner to outer are the impedimetric responses obtained at HRP/Chi-GAD/RuNPs/GCE for 5.92 x10^{-5} M–6.15 x 10^{-4} M H_2O_2 concentration additions. It is clear that the semicircle diameter is increasing with increase in H_2O_2 concentration additions. Similar results have been reported at other impedimetric sensors developed for glutamate [61], melamine [62] and Uranyl ion (UO_2^{2+}) determinations [63], in which they observed an increase in semicircle diameter while increasing melamine, glutamate and UO_2^{2+} concentrations, respectively. In the present study, the reason for the augmentation in semicircle diameter with increase in H_2O_2 concentrations could be attributed to the insulation layer formed by the adsorbed H_2O_2 at modified electrode surface which inhibits the charge transfer for the redox probe. However, only limited reports are available for H_2O_2 impedimetric biosensors [64]. In this cyt-C based impedimetric biosensor, the authors observed a decrease in semicircle diameter while increasing H_2O_2 concentration additions, but the reason for this type of behavior is not clear. On the other hand, Fig. 9 (a) represents the Randles equivalence circuit used to fit the experimental data. As explained in sec. 3. 5, the equivalence circuit parameters have their own meaning. By fitting the obtained experimental data with the Randles equivalence circuit, the R_{et} values have been calculated. As shown in Fig. 9 (b), a calibration curve was constructed by plotting the R_{et} values against the added H_2O_2 concentrations. From this calibration plot, the linear concentration range, correlation coefficient and sensitivity values are calculated as 5.92 x10^{-5} M–6.15 x 10^{-4} M, 0.9644 and 0.042 KΩ μM^{-1} cm^{-2}, respectively. It is notable that the linear H_2O_2 concentration range determined in this study is higher than the linear concentration range observed at cyt-C/α-COOH-PPy film and it is comparable to those reported at overoxidized polypyrrole (opPy) thin film based impedimetric sensors [65]. The good impedimetric H_2O_2 detection results achieved at the HRP/Chi-GAD/RuNPs film in this study could be attributed to the excellent biocompatibility of Chi-GAD film, good conductivity of RuNPs, and the good affinity of the composite film towards H_2O_2.

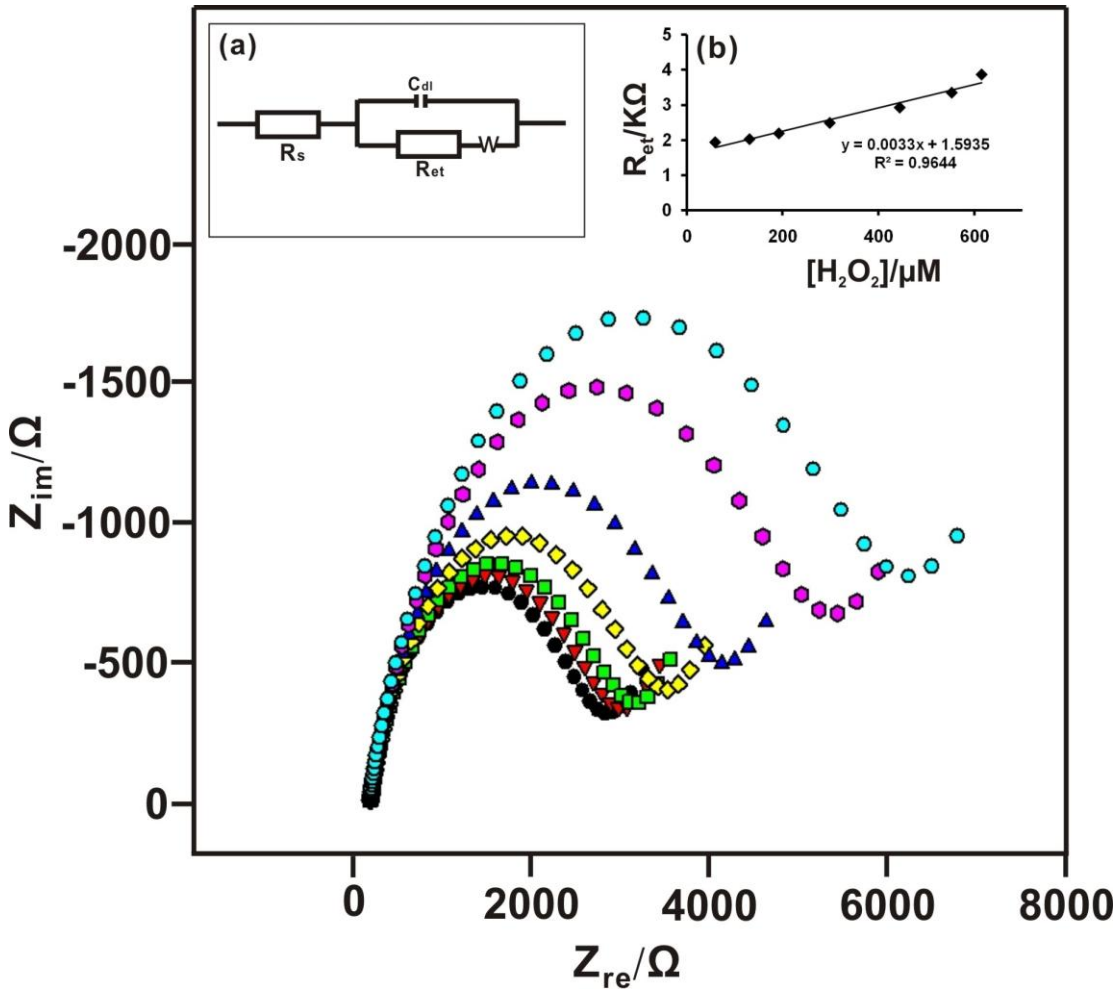

Figure 9. Impedimetric response obtained at HRP/Chi-GAD/RuNPs/GCE in presence of various H_2O_2 concentrations in PBS containing 5 mM $Fe(CN)_6^{3-}/Fe(CN)_6^{4-}$. The Nyquist plots from inner to outer were obtained after successive addition of 5.92 x10^{-5} M, 1.31 x 10^{-4} M, 1.92 x10^{-4} M, 2.98 x 10^{-4} M, 4.45 x 10^{-4} M, 5.53 x 10^{-4} M and 6.15 x 10^{-4} M H_2O_2 concentrations into the supporting electrolyte solution. Amplitude: 5 mV, frequency: 100 mHz to 100 kHz. Fig. 9 (a) is the Randles equivalence circuit used to fit the obtained EIS data and Fig. 9 (b) is the calibration plot which represents the linear dependence of R_{et}/KΩ vs. $[H_2O_2]$/μM.

3.6. Electrocatalytic detection of H_2O_2 at HRP/Chi-GAD/RuNPs film modified GCE

The electrocatalytic activity of HRP/Chi-GAD/RuNPs film modified GCE towards H_2O_2 has been investigated using CV experiments. Fig. 10 (a) shows the cyclic voltammogram obtained at HRP/Chi-GAD/RuNPs/GCE in the absence of H_2O_2. Whereas Fig. 10 (b-e) displays the cyclic voltammograms obtained at the same modified GCE after various H_2O_2 concentration additions. As shown in Fig. 10 (b) when 1.92 x 10^{-4} M of H_2O_2 was injected into the PBS, the composite film exhibits well-defined reduction peak at -0.273 V. This reduction peak current increased gradually with increase in H_2O_2 concentration additions ((Fig. 10 (b-e)). The composite film thus exhibits promising electrocatalytic activity towards H_2O_2 which could be attributed to the good biocompatibility of the

immobilized HRP as well as the synergistic effect of Chi-GAD/RuNPs matrix for H_2O_2. On the other hand, no obvious H_2O_2 reduction peak was observed at bare/GCE even in the presence of 7.80 x 10^{-4} M of H_2O_2, which signifies that bare/GCE has no catalytic activity for H_2O_2. Here it is noteworthy that, compared with the H_2O_2 reduction potential observed at bare/GCE (-0.6 V), HRP/Chi-GAD/RuNPs/GCE (-0.273 V) have lowered the reduction potential by 327 mV, validating the excellent electrocatalytic activity of the composite film.

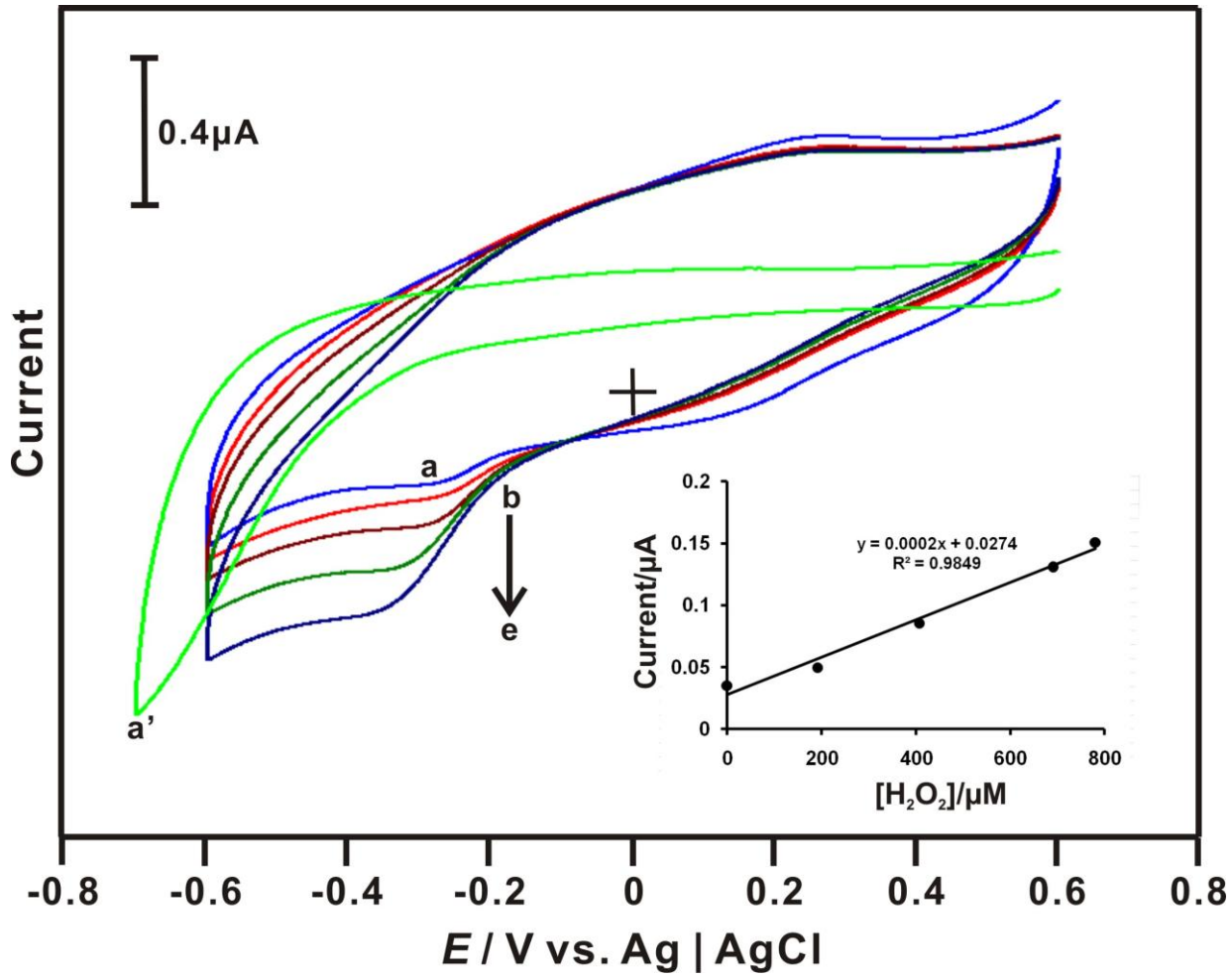

Figure 10. Cyclic voltamograms obtained at HRP/Chi-GAD/RuNPs film modified GCE at the scan rate of 20 mV s^{-1} in the absence (a) and presence of: (b) 1.92 x 10^{-4} M (c) 4.08 x 10^{-4} M (d) 6.91 x 10^{-4} M and (e) 7.80 x 10^{-4} M H_2O_2. Supporting electrolyte is N_2 saturated PBS. Inset is the plot of cathodic peak current vs. [H_2O_2].

The inset in Fig. 10 shows the calibration plot of I_{pc} vs. added H_2O_2 concentrations. From this calibration plot, the linear concentration range was obtained as 1.92 x 10^{-4} M–7.80 x 10^{-4} M H_2O_2, respectively. The S.D for five repetitive electrocatalytic measurements performed at the composite film for 4 x 10^{-4} M H_2O_2 additions is 2.8 which reveals the good repeatability of the proposed method for H_2O_2 quantification. Thus the composite film could be employed for repeated H_2O_2 quantifications. Furthermore, the composite film retains its background current even after 100 continuous CV potential

cycling scans were made in PBS between 0.6 V and -0.6 V (Figure not shown), which shows the good stability of the composite film. The good stability of the composite film could be attributed to the biocompatibility of Chi-GAD/RuNPs matrix and the covalent crosslinking between HRP and Chi-GAD.

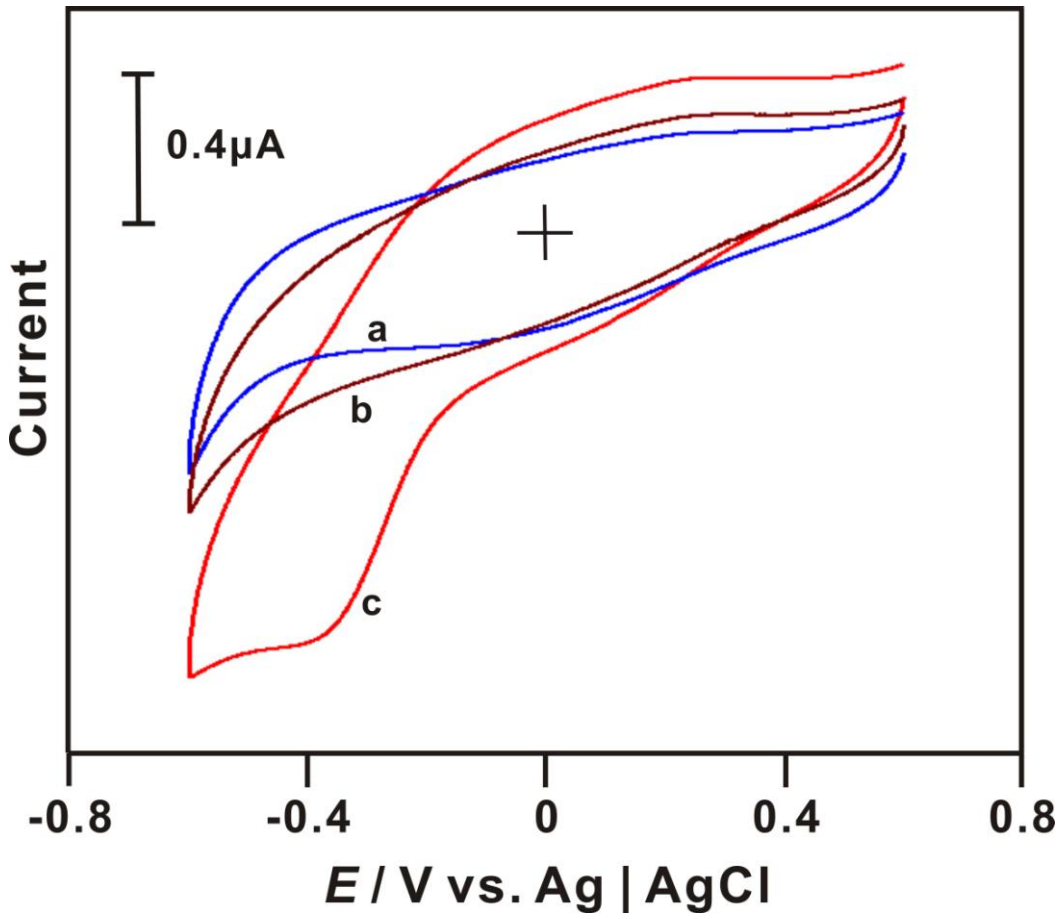

Figure 11. Cyclic voltamograms obtained at (a) RuNPs/GCE, (b) Chi-GAD/RuNPs/GCE and (c) HRP/Chi-GAD/RuNPs/GCE in the presence of 7.94 x 10^{-4} M of H_2O_2. The scan rate used: 20 mV s^{-1}.

Fig. 11(a-c) shows the cyclic voltammograms obtained at RuNPs, Chi-GAD/RuNPs and HRP/Chi-GAD/RuNPs film modified GCEs in the presence of 7.94 x 10^{-4} M of H_2O_2. In Fig. 11, compared with the catalytic reduction peak currents observed at RuNPs and Chi-GAD/RuNPs/GCEs, an enhanced reduction peak current has been observed at the HRP/Chi-GAD/RuNPs/GCE, validating the promising catalytic activity of the composite film surface. The electrocatalytic results obtained at different films manifests that composite film is more efficient for H_2O_2 reduction. The higher catalytic efficiency of the composite film could be ascribed to the good affinity of the immobilized HRP towards H_2O_2. In addition, the Chi-GAD layer present in the composite film helps to anchor the HRP at RuNPs modified electrode surface via covalent cross-linking. At the same time, the underlying

RuNPs layer acted as a good wiring between HRP and the GCE surface and it shuffled the electrons at a rapid rate.

3.7. Amperometric i-t curve studies at the composite film modified rotating GCE

The amperometric i-t curve study was investigated at HRP/Chi-GAD/RuNPs film modified rotating GCE in N_2 saturated PBS.

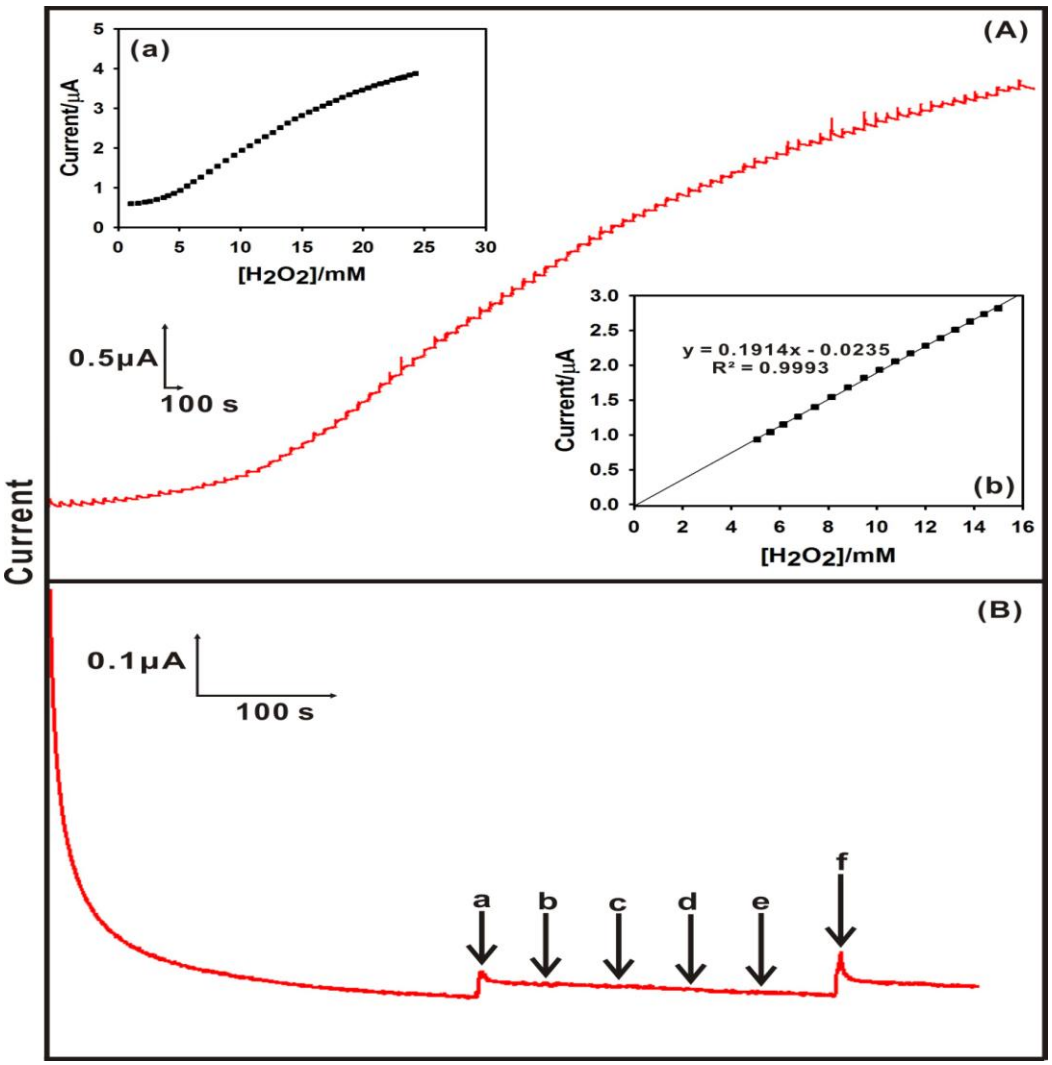

Figure 12. (A) Amperometric i-t response at HRP/Chi-GAD/RuNPs film modified rotating disc GCE upon successive additions of 1 x 10^{-5} M to 2.43 x 10^{-2} M H_2O_2 into continuously stirred N_2 saturated PBS. Applied potential: –0.3 V; Rotation rate: 900 RPM. The insets in (a) is the plot of response current vs. $[H_2O_2]$/mM (b) is the linear calibration plot obtained in the presence of 5.09 x 10^{-3} M–1.5 x 10^{-2} M H_2O_2. (B) Amperometric i-t response at HRP/Chi-GAD/RuNPs/GCE for the successive addition of (a) 100 µM H_2O_2 (b) 10 µM of AA, (c) 10 µM of UA, (d) 10 µM of L-Cysteine, (e) 10 µM of glucose and (f) 100 µM H_2O_2 into the same supporting electrolyte solution. The other experimental conditions are same as that of Fig. 12 (A).

During the amperometric experiments the electrode potential was held at –0.3 V and the N_2 saturated PBS was continuously stirred at 900 RPM. The H_2O_2 reduction potential (-0.3 V) at HRP/Chi-GAD/RuNPs film is much lower than the H_2O_2 reduction potentials reported at microspheres MnO_2/Nafion/GCE (0.8 V) [66] and it is slightly higher than the reduction potential reported at tin hexacyanoferrate Nanoparticles modified carbon ceramic electrode (-0.1 V) based amperometric H_2O_2 sensors [67]. Thus, HRP/Chi-GAD/RuNPs film considerably lowers the overpotential for H_2O_2 reduction and it could overcome the interfering signals resulting from the oxidation of the common interfering species. For every 50 s, aliquots of H_2O_2 were successively injected into the supporting electrolyte solution. Fig. 12 (A) shows the amperometric i-t response obtained at HRP/Chi-GAD/RuNPs composite film modified rotating disc GCE upon various H_2O_2 concentration additions. It is clear that, the composite film exhibits rapid, well-defined amperometric response towards each H_2O_2 concentration additions.

The response time of the HRP/Chi-GAD/RuNPs composite film towards H_2O_2 was 5 s, validating the rapid catalytic reduction process occurring at the composite film surface. The catalytic response current increases linearly between 5.09 x 10^{-3} M and 1.5 x 10^{-2} M H_2O_2 concentration additions as shown in the Fig. 12 (a). From the calibration plot shown in the Fig. 12 (b), the linear concentration range, correlation coefficient and the sensitivity values are calculated as 5.09 x 10^{-3} M– 1.5 x 10^{-2} M, 0.9993 and 0.798 μA mM^{-1} cm^{-2}, respectively. The linear H_2O_2 concentration range reported at HRP/Chi-GAD/RuNPs in this study is comparable to the linear H_2O_2 concentration range reported at ZnO–GNPs–Nafion–HRP film [26]. The satisfactory amperometric H_2O_2 determination results achieved at the HRP/Chi-GAD/RuNPs film in this study could be attributed to the good affinity of immobilized HRP for H_2O_2.

As shown in the Fig. 12 (a), the amperometric response curve exhibits a Michaelis menten behavior after 15 mM H_2O_2 concentration additions and it approaches a plateau for the H_2O_2 concentration range between 2 x 10^{-2} M and 2.43 x 10^{-2} M H_2O_2. This may be due to the reason that the enzyme activity has attained its saturation level at such high substrate concentrations. In order to study the enzyme kinetics as well as to evaluate the affinity of the immobilized HRP towards H_2O_2, the Michaelis–Menten constant (K_M^{app}) has been calculated from the electrochemical version of the Lineweaver–Burk equation given in eqn. (2) [68].

$$1/I_{ss} = 1/I_{max} + K_M^{app}/I_{max} \,.\, 1/C \qquad (2)$$

In the above equation, I_{ss} represents the steady state current measured after the addition of substrate, I_{max} is the maximum current measured under saturated substrate concentration, and C is the bulk concentration of substrate. From the plot of $1/I_{ss}$ vs. 1/C, the slope (K_M^{app}/ I_{max}) and the intercept ($1/I_{max}$) values are obtained as 2.8122 and 0.5556. Similarly, from these slope and intercept values, the I_{max} and K_M^{app} values are calculated as 1.7999 and 5.06 mM, respectively. The K_M^{app} value reported at HRP/Chi-GAD/RuNPs in this study is smaller than the K_M^{app} values reported at HRP-Fe_3O_4/CS-GCE (K_M^{app} =21. 4 mM) [69], HRP–SAM–Au electrode (K_M^{app} =6.34 mM) [70], HRP/Kieselguhr/PVA membrane-based H_2O_2 sensor (K_M^{app} == 572 mmol/L) [58]. The smaller K_M^{app} value obtained at HRP/Chi-GAD/RuNPs film indicates its high affinity towards H_2O_2. However, the K_M^{app} value

achieved in this study is higher than those reported at other nanostructured metal oxide modified HRP electrodes [26, 71]. This may be possibly due the change in the microenvironment of HRP at different nanostructured metal oxide matrices.

In order to determine H_2O_2 from real samples, the selectivity study is mandatory for the developed HRP based biosensor. It is well known that the biological fluids contain H_2O_2 along with the biomoloecules like ascorbic acid (AA), uric acid (UA), L-cysteine and glucose. Therefore, the selectivity of the developed HRP/Chi-GAD/RuNPs composite film was evaluated in the presence of these interfering species. The technique utilized for the selectivity study was amperometric i-t curve. In Fig. 12 (B), as indicated by (a), the fabricated HRP/Chi-GAD/RuNPs composite film showed rapid, well defined amperometric response towards 100 µM H_2O_2 addition. In contrast, when each 10 µM of AA, UA, L-cysteine and glucose solutions were successively injected into the same supporting electrolyte solution no notable amperometric response was observed as indicated by (b–e) in Fig.12 (B)). However, when 100 µM H_2O_2 was again injected into the same PBS an immediate amperometric response was observed (Fig. 12 (f)). The selectivity results thus confirmed that the proposed HRP biosensor is highly selective and it successfully overcomes the matrix effect caused by the common interferences, so it could be employed for the determination of H_2O_2 from real samples.

3.8. Real sample analysis

The practical applicability of HRP/Chi-GAD/RuNPs/GCE was investigated through real sample analysis. The technique used was amperometric i-t curve study. Commercially available contact lens cleaning solution was purchased from a local drug store in Taipei, Taiwan. The labeled composition of H_2O_2 present in the contact lens solution is 3 %. Further dilutions were made using PBS. During the amperometric experiments the working electrode potential was held at -0.3 V. The HRP/Chi-GAD/RuNPs modified rotating GCE showed excellent amperometric i-t response for the successive addition of H_2O_2 containing contact lens cleaning solution into PBS (Figure not shown). For every 50 s, $2x10^{-4}$ M H_2O_2 concentration was injected into the continuously stirring PBS. The amount of added, found H_2O_2 concentrations and recovery has been calculated for ten successive $2x10^{-4}$ M H_2O_2 concentration additions. The average recovery for ten successive H_2O_2 concentration additions is 91.3 %. The determination of H_2O_2 from commercially available contact lens cleaning solution with acceptable recovery reveals the good selectivity of the composite film towards H_2O_2 and the proposed biosensor could be employed for practical applications.

4. CONCLUSIONS

A highly selective amperometric and impedimetric biosensor for H_2O_2 detection has been developed using nanostructured RuO_2 film as a novel platform for HRP immobilization. For the first time, the direct electron transfer of HRP has been reported at the RuNPs modified electrode surface. HRP has been covalently immobilized at the RuNPs film surface via Chi-GAD crosslinking. The

immobilized HRP retains its native structure at the RuNPs matrix and exhibits good affinity towards H_2O_2. The proposed nanostructured metal oxide-HRP composite exhibits rapid response towards H_2O_2 in good linear concentration range, which could be ascribed to the synergistic effect of RuNPs for H_2O_2. The developed HRP/Chi-GAD/RuNPs film is highly selective towards H_2O_2 and satisfactory recovery results have been achieved in the contact lens cleaning solution, which validates the practical applicability of this method. The present study may encourage the exploitation of RuNPs as compelling matrices for probing the direct electron transfer of redox proteins.

ACKNOWLEDGEMENT
This work was supported by the National Science Council and the Ministry of Education of Taiwan (Republic of China).

References

1. S. Mueller, *Free Radical Biol. Med.*, 29 (2000) 410.
2. I.Slesak, M. Libik, B. Karpinska, S. Karpinski, and Z. Miszalski, *Acta Biochim. Pol.*, 54 (2007) 39.
3. C. K. Yeh, H. Wu, T. Chen, *J. Hazard. Mater.*, 96 (2003) 29.
4. R. J. Weston, *Food Chem.*, 71 (2000) 235.
5. D. B. Moore and D. S. Argyropoulos, *Anal. Chem.*, 71 (1999) 109.
6. R. Stolarek, P. Bialasiewicz, M. Krol, D. Nowak, *Clin. Chim. Acta*, 411 (2010) 1849.
7. T. Tatsuma, Y. Okawa, and T. Watanabe, *Anal. Chem.*, 61 (1989) 2352.
8. A.V. Jackson and C. N. Hewitt, *Atmos. Environ.*, 30 (1996) 819.
9. C. Xu and Z. Zhang, *Anal. Sci.*, 17 (2001) 1449.
10. C. Matsubara, K. Kudo, T. Kawashita and K. Takamura, *Anal. Chem.*, 57 (1985) 1107.
11. J. P. N. Ribeiro, M. A. Segundo, S. Reis, J. L. F. C. Lima, *Talanta*, 79 (2009) 1169.
12. Y. Woo, H. Lim, H. Kim, H. Chung, *J. Pharm. Biomed. Anal.*, 33 (2003) 1049.
13. T. Moreno, M. A. M. Lopez, I. H. Illera, C. M. Piqueras, A. S. Arranz, J. G. Serna, M. J. Cocero, *Chem. Eng. J.*, 166 (2011) 1061.
14. S. Ledru, N. Ruille, M. Boujtita, *Biosens. Bioelectron.*, 21 (2006) 1591.
15. J. Wang, L. Wang, J. Di, Y. Tu, *Talanta*, 77 (2009) 1454.
16. S.V. Dzyadevych, V. N. Arkhypova, A. P. Soldatkin, A. V. Elskaya, C. Martelet , N. Jaffrezic-Renault, *ITBM-RBM*, 29 (2008) 171.
17. H. Li, S. Liu, Z. Dai, J. Bao and X. Yang, *Sensors*, 9 (2009) 8547.
18. H. Yin, S. Ai, W. Shi, L. Zhu, *Sens. Actuators, B*, 137 (2009) 747.
19. J. Xu, F. Shang, J. H. T. Luong, K. M. Razeeb, J. D. Glennon, *Biosens. Bioelectron.*, 25 (2010) 1313.
20. Z. Zhu, X. Li, Y. Wang, Y. Zeng, W. Sun, X. Huang, *Anal. Chim. Acta*, 670 (2010) 51.
21. Y. Yang, G. Yang, Y. Huang, H. Bai, X. Lu, *Colloids Surf., A*, 340 (2009) 50.
22. S. Wang, F. Xie, G. Liu, *Talanta*, 77 (2009) 1343.
23. Md. M. Rahman, A. J. S. Ahammad, J. Jin, S. J. Ahn and J. Lee, *Sensors*, 10 (2010), 4855.
24. A.Liu, *Biosens. Bioelectron.*, 24 (2008) 167.
25. Y. Zhang, Y. Zhang, H. Wang, B. Yan, G. Shen, R. Yu, *J. Electroanal. Chem.*, 627 (2009) 9.
26. C. Xiang, Y. Zou, L. X. Sun, F. Xu, *Sens. Actuators, B*, 136 (2009) 158.
27. Y. Wang, X. Ma, Y. Wen, Y. Xing, Z. Zhang, H. Yang, *Biosens. Bioelectron.*, 25 (2010) 2442.
28. Y. Astuti, E. Topoglidis, A. G. Cass, J. R. Durrant, *Anal. Chim. Acta*, 648 (2009) 2.
29. J. Liu, Y. Li, X. Huang, Z. Zhu, *Nanoscale Res. Lett.*, 5 (2010) 1177.
30. P. He, N. Hu, *Electroanal.*, 16 (2004) 1122.

31. A. A. Ansari, P. R. Solanki, B. D. Malhotra, *J. Biotechnol.*, 142 (2009) 179.
32. A.Mohammadi, A. B. Moghaddam, M. Kazemzad, R. Dinarvand, J. Badraghi, *Mater. Sci. Eng., C,* 29 (2009) 1752.
33. X. Yang, X. Chen, X. Zhang, W. Yang, D. G. Evans, *Sens. Actuators, B,* 134 (2008) 182.
34. S. Zong, Y. Cao, Y. Zhou and H. Ju, *Langmuir,* 22 (2006) 8915.
35. X. Yang, X. Chen, L. Yang, W. Yang, *Bioelectrochem.,* 74 (2008) 90.
36. X. Kang, J. Wang, Z. Tang, H. Wu, Y. Lin, *Talanta,* 78 (2009) 120.
37. N. Jia, Q. Zhou, L. Liu, M. Yan, Z. Jiang, *J. Electroanal. Chem.,* 580 (2005) 213.
38. F. Wu, Z. Hu, L. Wang, J. Xu, Y. Xian, Y. Tian and L. Jin, *Electrochem. Commun.,* 10 (2008) 630.
39. A.Radi, X. Munoz-Berbel, M. Cortina-Puig, J. Marty, *Electroanal.,* 21 (2009) 696.
40. B. Krajewska, *Enzyme Microb. Technol.*, 35 (2004) 126.
41. X. Zhao, Z. Mai, X. Kang, X. Zou, *Biosens. Bioelectron.,* 23 (2008) 1032.
42. D. Shan, Q. Li, S. Ding, J. Xu, S. Cosnier, H. Xue, *Biosens. Bioelectron.,* 26 (2010) 536.
43. V. Crescenzi, A. Francescangeli, A. Taglienti, D. Capitani, and L. Mannina, *Biomacromolecules*, 4 (2003) 1045.
44. J. C. Chou, Y. H. Tsai, and C. C. Chen, *IEEE Sens. J.* 8 (2008) 1571.
45. Y. Peng, G. Yi and Z. Gao, *Chem. Commun.*, 46 (2010) 9131.
46. P. Kotzian, P. Brazdilova, K. Kalcher, K. Vytras, *Anal. Lett.,* 38 (1099–1113) 2005.
47. O. A.C. Monteiro Jr., C. Airoldi, *Int. J. Biol. Macromol.*, 26 (1999) 119.
48. C. C. Hu, Y. H. Huang, *J. Electrochem. Soc.* 146 (1999), 2465.
49. P. Shakkthivel, S.M. Chen, *Biosens. Bioelectron.,* 22 (2007) 1680.
50. S. M. Chen, S. H. Hsueh, *J. Electroanal. Chem.,* 566 (2004) 291.
51. J. Hong, A. A. M. Movahedi, H. Ghourchian, A. M. Rad, S. R. Zarchi, Electrochim., Acta, 52 (2007) 6261.
52. F. Li, Y. Feng, Z. Wang, L. Yang, L. Zhuo, B. Tang, *Biosens. Bioelectron.,* 25 (2010) 2244.
53. Y. Xu, C. Hu, S. Hu, *Anal. Chim. Acta*, 663 (2010) 19.
54. J. Z. Xu, J. J. Zhu, Q. Wu, Z. Hu, H. Y. Chen, *Electroanal.,* 15(2003) 219.
55. Y. T. Kong, M. Boopathi, Y. B. Shim, *Biosens. Bioelectron.,* 19 (2003) 227.
56. J. S. Long, D. S. Silvester, G. G. Wildgoose, A. E. Surkus, G. Flechsig, R. G. Compton, *Bioelectrochem.*, 74 (2008) 183.
57. R. Yan, F. Zhao, J. Li, F. Xiao, S. Fan, B. Zeng, *Electrochim. Acta,* 52 (2007) 7425.
58. C. Fan, H. Wang, D. Zhu, G. Wagner, and G. Li, *Anal. Sci.* 17 (2001) 273.
59. X. Yang, X. Chen, L. Yang, W. Yang, *Bioelectrochem.* 74 (2008) 90.
60. X. Chen, X. Peng, J. Kong, J. Deng, *J. Electroanal. Chem.,* 480 (2000) 26.
61. R. Maalouf, H. Chebib, Y. Saikali, O. Vittori, M. Sigaud, N. J. Renault, *Biosens. Bioelectron.,* 22 (2007) 2682.
62. T. H. Tsai, S. Thiagarajan, and S. M. Chen, *J. Agric. Food Chem.* 58 (2010) 4537.
63. R. K. Shervedani, S. A. Mozaffari, *Anal. Chim. Acta*, 562 (2006) 223.
64. M. Shamsipur, S. H. Kazemi, M. F. Mousavi, *Biosens. Bioelectron.,* 24 (2008) 104.
65. D. Zane, G. B. Appetecchi, C. Bianchini, S. Passerini, A. Curulli, *Electroanal.,* 22 (2010).
66. L. Zhang, Z. Fang, Y. Ni, G. Zhao, *Int. J. Electrochem. Sci.*, 4 (2009) 407.
67. H. Razmi, A. Taghvimi, Int. J. Electrochem.Sci., 5 (2010) 751.
68. R. A. Kamin, G. S. Willson, *Anal. Chem.* 52 (1980), 1198.
69. X. Tan, J. Zhang, S. Tan, D. Zhao, Z. Huang, Y. Mi, Z. Huang, *Electroanal.* 21 (2009) 1514.
70. Y. Yang, M. Yang, H. Wang, J. Jiang, G. Shen, R. Yu, *Sens. Actuators, B,* 102 (2004) 162.
71. F. Wu, J. Xu, Y. Tian, Z. Hu, L. Wang, Y. Xian, L. Jin, *Biosens. Bioelectron.,* 24 (2008) 198.

© 2011 by ESG (www.electrochemsci.org)